Heliyon 9 (2023) e22277

Contents lists available at ScienceDirect

Heliyon

journal homepage: www.cell.com/heliyon

Study on the fluidity of foamed alkali-activated slag cementitious material (AASCM)

Kunpeng Yu [a], Liqiang Ma [a,b,*], Ichhuy Ngo [a], Yangyang Wang [a], Jiangtao Zhai [a]

[a] School of Mines, China University of Mining and Technology, Xuzhou, 221116, China
[b] Key Laboratory of Xinjiang Coal Resources Green Mining (Xinjiang Institute of Engineering), Ministry of Education, Urumqi 830023, China

ARTICLE INFO

Keywords:
Foamed backfill
Fluidity
Foaming agent dosage
Particle size of filling aggregate
Water film thickness

ABSTRACT

This study aims to investigate the evolution patterns of fluidity and rheological properties of AASCM under varying dosages of foaming agent and particle sizes of filling aggregate. The flow characteristics of AASCM are significantly affected by the filling aggregate's size and the foaming agent's dosage. Specifically, an increase in filling aggregate size (D(4,3) ϵ [26 μm, 69 μm]) enhances the fluidity of foamed AASCM, while an increase in foaming agent dosage reduces fluidity. These observed variations can be attributed to the presence of particle voids, the specific surface area of the aggregate, as well as the quantity and spatial distribution of bubbles within the slurry. A bubble-particle packing model is established, and by calibrating the simulation error coefficient to 1.1, the study investigates the evolution of water film thickness (WFT) in foamed AASCM with slurry expansion degree. It is observed that bubbles in the slurry affect the fluidity by altering the overall compactness and specific surface area of the foamed slurry, subsequently modifying the WFT.

1. Introduction

As economic development continues to grow, the concrete and cement industry faces ongoing environmental challenges on a global scale [1,2]. Portland cement production is resource-intensive and can have environmental impacts, including the emission of greenhouse gases. Efforts are being made to develop more sustainable alternatives and reduce the environmental footprint of cement production [3–5]. Therefore, low-carbon materials are increasingly being emphasized worldwide. It is urgently needed to develop alternative binders to replace Portland cement [6]. Alkali-activated slag cementitious material (AASCM) is a binder that exhibits strength similar to Portland cement. AASCM is a green low-carbon cementitious material generated by reacting alkaline activators with slag that has potential hydraulic activity [7]. It not only has simple reaction conditions but also exhibits several desirable properties such as high strength, impermeability, resistance to acids and alkalis, frost resistance, as well as high-temperature resistance [8]. AASCM is a potential substitute for cement [9,10]. This material has the advantages of a simple production process, no need for calcination, low cost, low energy consumption, low carbon footprint, maintaining ecological balance, environmental friendliness, and achieving large-scale resource recycling of solid waste [11,12]. It is an advanced green material with enormous development potential. The carbon emission per kilogram of AASCM produced is approximately one-fifth that of ordinary Portland cement [13,14]. Meanwhile, the production process of AASCM incorporates a significant quantity of industrial solid waste, leading to enhanced resource utilization, environmental improvement, and the advancement of the circular economy. As a result, AASCM has garnered considerable

* Corresponding author.
E-mail address: tbh275@cumt.edu.cn (L. Ma).

https://doi.org/10.1016/j.heliyon.2023.e22277
Received 13 June 2023; Received in revised form 9 October 2023; Accepted 8 November 2023
Available online 14 November 2023

attention from numerous scholars as an environmentally friendly material. In decades of development, numerous research achievements have been made in the preparation process, influencing factors, hydration mechanism, workability, and durability of AASCM [15–17]. Numerous researchers have conducted comprehensive assessments of the research advancements concerning AASCM [18–22].

In recent years, backfill mining has been recognized as an effective and environmentally friendly mining technique, leading the development direction of waste-free, green, and safe mining in the mining industry. Currently, backfill mining technology involves processing solid waste materials, including coal mining gangue and power plant fly ash, industrial slag, and other solid waste into slurry-like backfill materials on the ground [23–27]. Dedicated backfill pumps and pipelines are used to transport the backfill materials to the underground working face. During the consolidation process of the backfill material, solid particles settle, forcing excess water out, leading to a decrease in the overall volume of backfill material required. This phenomenon is manifested in the difficulty of achieving complete backfill coverage [28,29]. In this case, the stability of the overlying roof under large loads cannot be guaranteed, which is detrimental to large-scale mechanized operations and can cause subsidence of the surface in the overall mining area. Given the drainage and self-shrinking characteristics of traditional backfill materials, it is proposed to add a foaming agent to the backfill slurry to create a porous structure, control the expansion rate, ensure that the backfill material is in close contact with the roof, and provide the strength required to maintain the stability of the mining area. Compared with ordinary backfill materials, increasing the self-expansion performance of the backfill material can reduce volume shrinkage. Therefore, it is feasible to prepare backfill materials with expansion characteristics to improve backfill coverage. Therefore, the study of foamed backfill technology is of great significance to optimize the utilization of solid waste generated from mining operations, controlling surface subsidence, and improving backfill efficiency.

As is widely recognized, the fluidity of filling slurry profoundly influences the efficiency of pipeline transportation. The fluidity of the slurry is often characterized by its expansion degree, and extensive research has been conducted by scholars [30–34]. For the unfoamed filling slurry, the main factors affecting its fluidity include temperature, binder content, solid particle size, solid mass concentration, mineral additives, and chemical additives [35–37]. However, there are relatively few studies have been conducted on the fluidity of foamed AASCM, and the mechanisms underlying its effects on fluidity are not yet clear. The study of the flow properties and stability of alkali-activated materials containing foaming agents is an important topic in the fields of construction and materials science, particularly in areas such as underground mining, tunnel construction, and infrastructure development [6,7]. AASCM are commonly used in underground backfilling materials, making their flow properties of paramount importance [25]. Flow properties determine the material's ability to flow during the filling or backfilling process, which is crucial for ensuring complete filling of voids and avoiding the formation of gaps and voids [26]. The application of foaming agents in alkali-activated materials can enhance their flow properties [6]. Foaming agents can introduce air bubbles or porous structures, reducing the material's density and thus improving its flowability. This is particularly important for achieving uniform filling in underground engineering [7]. In underground engineering, the stability of filling or backfill materials is a critical concern. If the material cannot maintain its stability after filling, it can lead to geological hazards such as collapse or landslides [29]. Therefore, it is essential to ensure that alkali-activated materials containing foaming agents remain stable after filling and do not collapse due to external pressures or other factors. The composition and proportions of the materials are crucial for both flow properties and stability [18,19]. The right formulation can ensure that the material has sufficient flowability while maintaining the necessary strength and stability to meet specific engineering requirements [20]. To better understand the flow properties and stability of alkali-activated materials containing foaming agents, experimental research and numerical simulation analysis are typically conducted [21,22]. These studies can help determine the optimal material combinations and engineering parameters. In summary, research on the flow properties and stability of alkali-activated materials containing foaming agents is a significant area of study, addressing critical issues in underground engineering and infrastructure development.

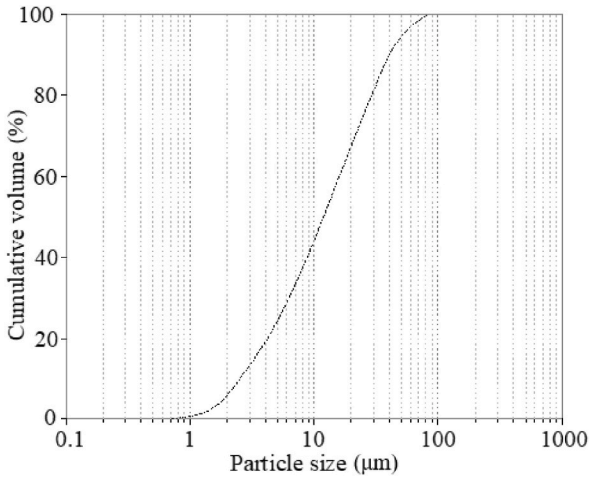

Fig. 1. The size distribution of particles in GGBFS.

Motivated by the discussion mentioned above, this paper mainly focuses on studying the impacts of foaming agent dosage and aggregate gradation on the flow characteristics of AASCM samples. To achieve this goal, circulating fluidized bed combustion fly ash (CFA) and both coarse and fine grain size gangue (CG and FG) were adopted to prepare AASCM mixtures with various aggregate gradations (11 gradations with volume moment mean between 26 and 69 μm) and foaming agent dosages (0∼2.8 %). Parameters for fresh AASCM (fluidity, water film thickness (WFT), and expansion ratio) were compared as a function of aggregate gradation and foaming agent dosage. The findings of this research offers a theoretical foundation for the engineering application of foamed filling in mines.

2. Materials

2.1. Binders

The binder chosen for the study was alkaline-activated S95-grade ground granulated blast furnace slag (GGBFS). A high-purity sodium silicate with a 99.9 % purity level served as the alkaline activator. The distribution of particle sizes of the slag was analyzed through the application of laser-based particle size analysis, and the corresponding results are presented in Fig. 1. The D_{50} of the slag was 13.18 μm, the uniformity coefficient was 8.25, the curvature coefficient was 1.03, and the uniformity coefficient was 2.36, indicating a good particle size distribution. The GGBFS was subjected to physicochemical and mineralogical analyses. Table 1 and Fig. 2 present the elemental and mineral compositions of the GGBFS determined by X-ray fluorescence (XRF, Bruker model S8 Tiger spectrometer, Germany) and X-ray diffraction (XRD, Bruker model D8 Advance, Germany), respectively. Qualitative analysis using XRF (X-ray fluorescence) spectroscopy revealed that the primary composition (mass fraction) of the slag was 9.927 % MgO, 16.261 % Al_2O_3, 29.917 % SiO_2, and 36.978 % CaO. The XRD (X-ray diffraction) analysis of the mineral phases, as depicted in Fig. 2, reveals the presence of a prominent "dispersion peak" in the slag XRD pattern within the diffraction angle range of 25°–35°. This indicates that the mineral phase composition of the slag micro-powder still contains amorphous material in the form of glass phase, along with crystalline phases of minerals such as quartz (SiO_2), calcium aluminum pyroxene ($Ca_2Al_2SiO_7$), and magnesium pyroxene ($Ca_2MgSi_2O_7$).

2.2. Filling aggregate

To investigate the impact of various aggregate size distributions on the fluidity of foamed filling slurries, low-calcium grade I fly ash from circulating fluidized bed combustion (CFA) was selected and mixed with two sizes of gangue (coarse and fine) to form various mixtures of aggregate size distributions as shown in Fig. 3(a). The specific proportions are shown in Table 2. Following the uniform blending of the components based on the ratios provided in the table, the particle size distribution of the resulting aggregate was depicted in Fig. 3(b). The figure demonstrates that an increased proportion of fine gangue leads to a finer particle size distribution of the mixed aggregate, while a higher proportion of coarse gangue results in a coarser particle size distribution of the mixed aggregate. To effectively characterize the level of coarseness observed in the mixed aggregate size distribution, characteristic parameters of particle size distribution were used, including D_{20}, D_{50}, D_{80}, curvature coefficient (C_c), and uniformity coefficient (C_u). Although these parameters can describe the particle size distribution and grading well, there is too much data to analyze. Therefore, assuming the particles are ideal spheres. To provide a statistical description of the particle size distribution, the average particle size was determined, represented by $D(4,3)$. Table 3 presents the different particle size characteristic parameters for the 11 aggregates.

2.3. Foaming agent

The foaming agent used in this study was a 30 % concentration solution of hydrogen peroxide. To minimize the sensitivity of the foaming agent to the experimental data, the 30 % hydrogen peroxide solution should be added after uniformly stirring the slurry and then stirred uniformly for 30 s. It should be noted that the stirring speed and time used for each preparation of foamed filling slurry are the same, and the indoor temperature is controlled within ±2 °C.

3. Experimental methodologies

3.1. Test scheme

To investigate the impact of varying dosages of foaming agent on the flow characteristics of foamed backfill slurries, referring to relevant references on foaming materials [38,39] and preliminary experiments, the foaming agent dosage was tentatively set as 0 %, 0.7 %, 1.5 %, 2.3 %, and 3.1 % of the mass of the binder while controlling the expansion rate of the foamed filling body to be less than 15 %. The experimental setup details are presented in Table 4.

Table 1
Oxide compositions of GGBFS (in %).

Sample	MgO	Al_2O_3	SiO_2	CaO	LOI
GGBFS	9.927	16.261	29.917	36.978	6.917

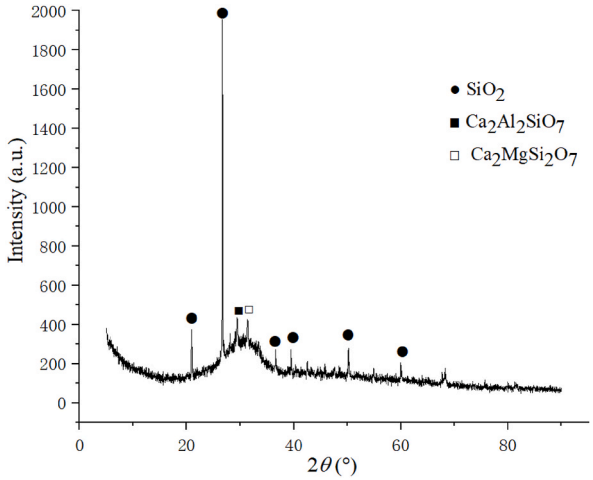

Fig. 2. The XRD patterns of GGBFS.

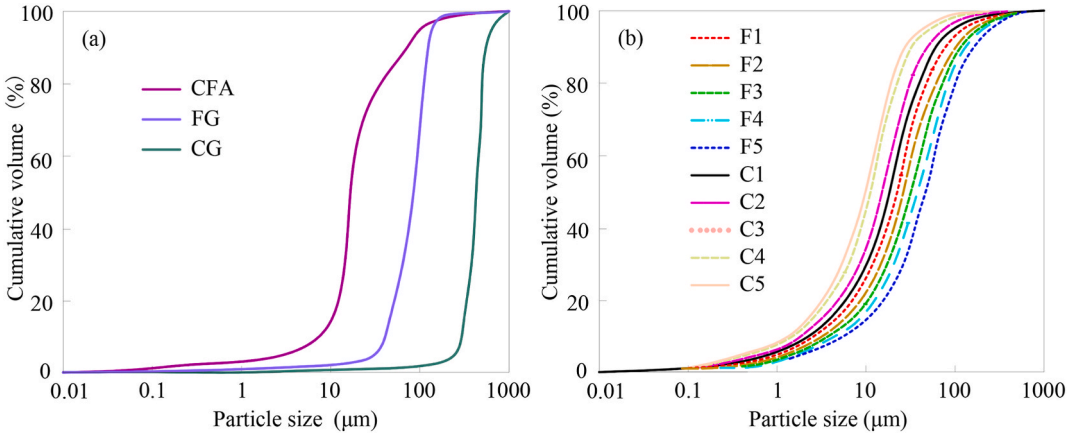

Fig. 3. The distribution of particle sizes in the CFA, the FG, the CG, and mixed aggregates.

Table 2
Mix ratios for the CFA and gangue (mass fraction).

No.	CFA/%	Fine/%	Coarse/%
CFA	100	–	–
F1	90	10	–
F2	80	20	–
F3	70	30	–
F4	60	40	–
F5	50	50	–
C1	90	–	10
C2	80	–	20
C3	70	–	30
C4	60	–	40
C5	50	–	50

For slurries with the same concentration and foaming agent dosage, different aggregate particle sizes can significantly affect the flow properties of the slurry due to the large difference in overall solid bulk density. Foamed filling slurries were prepared using the 11 types of aggregate particle sizes listed in Table 2, with foaming agent dosages of 0 %, 0.7 %, 1.4 %, 2.1 %, and 2.8 % (by mass fraction of binder), a ratio of fly ash to sand at 0.25, with a solid mass concentration of 74 %. A comprehensive outline of the experimental design is provided in Table 5.

Table 3
Particle parameters of mixed aggregates.

No.	D_{20}/ μm	D_{50}/ μm	D_{80}/ μm	C_u	C_c	n	P	$D(4,3)$/μm
CFA	10.62	16.86	38.31	3.435	1.186	0.9052	0.581	26.27
F1	10.78	18.21	39.43	2.886	1.021	0.8706	0.578	27.31
F2	10.94	21.04	43.06	3.201	1.010	0.8785	0.571	28.19
F3	11.25	24.65	46.97	3.411	1.013	0.9006	0.567	30.67
F4	11.43	27.10	50.67	3.397	1.009	0.8914	0.560	31.69
F5	11.71	29.92	55.12	2.702	1.152	0.9052	0.554	33.58
C1	11.21	21.68	59.68	2.515	1.008	0.8259	0.578	38.24
C2	12.36	25.84	64.21	2.327	1.016	0.8208	0.589	45.07
C3	14.06	29.37	68.58	2.211	1.030	0.8007	0.596	53.01
C4	15.67	35.61	73.17	2.189	1.021	0.7946	0.608	61.57
C5	17.20	42.79	77.16	2.068	1.009	0.7835	0.606	69.05

Note: P represents the aggregate's bulk density, while n is an invariable associated with the distribution breadth of particle size. The value of n is inversely proportional to the breadth of the particle size distribution.

Table 4
Influence of foaming agent dosage on the fluidity of fresh AASCM.

No.	GGBFS-CFA ratio	Cementing agent	Filling aggregate	Solid particle concentration/%	Foaming agent dosage/%
1	0.25	Alkali-activated slag	CFA	67,71,74,77	0
2	0.25	Alkali-activated slag	CFA	67,71,74,77	0.7
3	0.25	Alkali-activated slag	CFA	67,71,74,77	1.4
4	0.25	Alkali-activated slag	CFA	67,71,74,77	2.1
5	0.25	Alkali-activated slag	CFA	67,71,74,77	2.8

3.2. Material testing

3.2.1. Slump test

The slump test reflects the cohesion and frictional resistance of the filling material and is an important indicator for measuring fluidity. Due to the low solid mass concentration and fine aggregate size of the fill slurry, the conventional slump test is a time-intensive process that necessitates a substantial quantity of material. Therefore, the Mini-Slump test is gradually being used by many researchers to assess the flow characteristics of the backfill slurry [40,41]. In the Mini-Slump test, the fluidity of the backfill slurry is commonly quantified using the flow spread diameter (degree of spreading). The flow spread diameter is influenced by the yield stress, which directly affects the conveying efficiency of the slurry through pipelines. For the test, a Mini-Slump cone with a top diameter of 50 mm, a bottom diameter of 100 mm, and a height of 150 mm was employed. According to the ASTM-C143 standard [42], the fluidity test is carried out by pouring the uniformly stirred slurry into the slump cone, compacting it, lifting it vertically for 2 min, and measuring the spread diameter in any two vertical directions. The average of the two is taken as the index of the fluidity of the fill slurry. The experiment was conducted in triplicate, and the average slump value was obtained for subsequent analysis.

3.2.2. Viscosity measurement

Bingham yield stress and plastic viscosity are commonly used indicators to characterize the rheological properties of newly made fill slurry [43]. In this paper, these two indicators are also used to evaluate the rheological characteristics of newly made foamed fill slurry. The plastic viscosity is calculated by dividing the shear stress exerted on the fluid by the shear rate [44]. Being a non-Newtonian fluid, the plastic viscosity of freshly prepared foamed fill slurry varies with the shear rate. In this study, the plastic viscosity of the foamed fill slurry was measured using an NDJ-8S rotary viscometer equipped with a No.3 rotor. The viscometer has a measuring range

Table 5
Influence of varying particle sizes of filling aggregate on the fluidity of fresh AASCM.

No.	GGBFS-CFA ratio	Cementing agent	Solid particle concentration/%	Foaming agent dosage/%
CFA	0.25	Alkali-activated slag	74	0,0.7,1.4,2.1,2.8
F1	0.25	Alkali-activated slag	74	0,0.7,1.4,2.1,2.8
F2	0.25	Alkali-activated slag	74	0,0.7,1.4,2.1,2.8
F3	0.25	Alkali-activated slag	74	0,0.7,1.4,2.1,2.8
F4	0.25	Alkali-activated slag	74	0,0.7,1.4,2.1,2.8
F5	0.25	Alkali-activated slag	74	0,0.7,1.4,2.1,2.8
C1	0.25	Alkali-activated slag	74	0,0.7,1.4,2.1,2.8
C2	0.25	Alkali-activated slag	74	0,0.7,1.4,2.1,2.8
C3	0.25	Alkali-activated slag	74	0,0.7,1.4,2.1,2.8
C4	0.25	Alkali-activated slag	74	0,0.7,1.4,2.1,2.8
C5	0.25	Alkali-activated slag	74	0,0.7,1.4,2.1,2.8

of 1~2 × 10^6 mPa s, and a speed of 30 r/min.

Regarding the Bingham yield stress, it represents the static yield stress of the material. A higher Bingham yield stress indicates enhanced solidification characteristics of the slurry [45]. When the shear stress exerted on the freshly prepared foamed fill slurry surpasses the Bingham yield stress, visible flow is observed. In this study, a self-made Bingham yield stress testing device, illustrated in Fig. 4 (a) [46], was utilized to measure the Bingham yield stress. The measured Bingham yield stress is referred to as the equivalent Bingham yield stress.

During the test, the pulling force is measured using a precision of 0.001 N tensile force gauge, and the thin plastic plate embedded in the newly made foamed fill slurry has a size of 50 mm wide and 75 mm high. Four measurements are taken at different positions of each newly made foamed fill slurry sample, as shown in Fig. 4 (b), and the average of the four measurements is taken as the equivalent Bingham yield stress. The specific calculation formula can be expressed as:

$$\tau_m = \frac{F_1 + F_2 + F_3 + F_4}{8bh}$$

in the formula, F_1, F_2, F_3 and F_4 are the tension values tested at the four positions respectively, N. b represents the width of the thin plate, mm. h represents the depth of the sheet embedded in the paste, mm. τ_m as the equivalent yield stress, Pa or N/m^2.

3.2.3. Bulk density

The method of measuring bulk density can be categorized into two groups: dry stacking and wet stacking methods. The dry stacking method is heavily influenced by the degree of compression, and to avoid this issue, the wet stacking method is utilized in this study for measuring the bulk density of the foamed filling slurry [47]. The fundamental principle of the wet stacking method involves incorporating different quantities of water into the solid particles, where the solid particle concentration first increases and then decreases, and the bulk density is determined based on the maximum solid particle concentration. At low water content, numerous liquid bridges are formed, resulting in a reduced distance between solid particles. As a consequence, the solid particle concentration tends to increase [48]. However, with an increase in water content, the particles become more dispersed, leading to an expansion in the volume of the slurry, resulting in a decrease in the solid particle concentration [49].

4. Results and discussion

4.1. Influence of foaming agent dosage on the volumetric expansion and rheological characteristics of fresh AASCM

The impact of foaming agent dosage on the slurry expansion is depicted in Fig. 5. The data indicates an inverse relationship between the escalation of foaming agent dosage and the change in slurry expansion. For instance, for foam filling slurry with a solid particle concentration of 74 %, with the foaming agent dosage ranging from 0 % to 2.8 %, the expansion decreases from 246 mm to 219 mm, a reduction of 27 mm. This phenomenon can be attributed to a rise in the bubble population within the slurry as the foaming agent dosage increases. When bubbles are stable inside the slurry, a film is formed on their surface that consists of water mixed with solid particles, including filling aggregates and binding agents. With an increase in the number of bubbles, the surface area expands, necessitating a certain portion of free water to be distributed among the bubbles for maintaining their stable configuration [50,51]. As a consequence, the availability of free water for the slurry to flow decreases, leading to a reduction in slurry expansion. Moreover, it was observed that different solid particle concentrations correspond to different changes in expansion as foaming agent dosage increases from 0 % to 2.8 %. For the same solid particle concentration, the extent of the decrease in expansion varies with increasing foaming agent dosage and generally exhibits a decreasing trend. For example, for foam filling slurry with a solid particle concentration of 77 %, the reduction in expansion is 15.1 mm, 10.1 mm, 9.2 mm, and 0.2 mm, respectively, with the foaming agent dosage progressively increasing from 0 % to 0.7 % and further to 2.8 %. This indicates that a foaming agent dosage of 2.8 % or higher exerts a comparatively lesser influence on the fluidity of higher solid particle concentration (77 %) slurry. This can be attributed to the higher

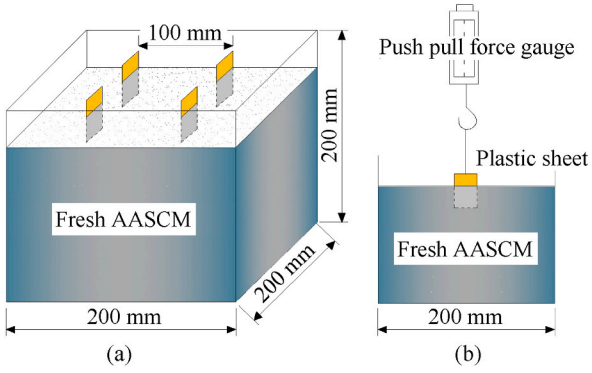

Fig. 4. Device for measuring the equivalent Bingham yield stress of fresh AASCM.

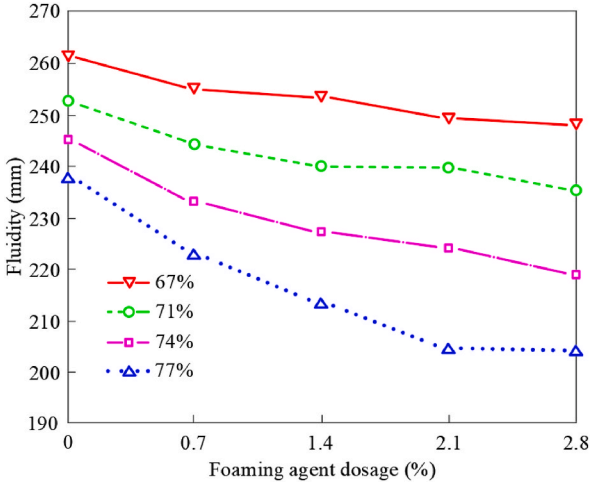

Fig. 5. Influence of foaming agent dosage on the flow properties of fresh AASCM.

viscous behavior and Bingham yield strength of the higher solid particle concentration (77 %) slurry, which makes it difficult for bubbles to move, expand, and fuse, thereby maintaining their distribution state stable. On the other hand, the adhesion between solid particles and bubbles increases with higher foaming agent dosage, causing the increase in the stiffness of fresh AASCM and then the decrease in the fluidity [52].

The rheological characteristics of foamed slurry as influenced by the foaming agent dosage are depicted in Fig. 6. As observed from the figure, a rise in the dosage of foaming agent is directly proportional to the changes in the rheological properties of the foamed slurry. For instance, for a foamed slurry with a solid particle concentration of 74 %, with the foaming agent dosage ranging from 0 % to 2.8 %, the effective Bingham yield strength of the foamed slurry experiences an increase from 32.6 Pa to 45.7 Pa, resulting in an increment of 13.1 Pa, while the exhibits an increase from 0.57 Pa s to 0.93 Pa s in plastic viscosity, resulting in an increment of 0.36 Pa s. With the increase in foaming agent dosage, the number of bubbles rises, thereby influencing the bulk density of the foamed slurry. The gaps between bubbles and solid particles increase, and for a constant water content, more free water is absorbed to fill the gaps [51]. Additionally, the total surface area of the foamed slurry increases, which also requires more free water to reduce the interfacial forces between the solid particles and bubbles, leading to a reduction in the fluidity of the slurry, making it difficult to shear and increasing its viscosity. Moreover, previous studies [32,53,54] have shown that the flow characteristics of the slurry are closely linked to its rheological properties, as an increase in fluidity leads to a corresponding increase in rheological parameters.

4.2. *Effects of aggregate size on the expansion and rheological characteristics of freshly prepared AASCM*

As indicated by the particle size parameters of the foamed filling aggregates in Table 2, with an increase in the proportion of coarse aggregates, the volume mean diameter $D(4,3)$ exhibited an upward trend, while a decrease in the proportion of fine aggregates resulted in a decrease in the volume mean diameter $D(4,3)$. An increase in the proportion of coarse aggregates led to a decrease in the bulk density P, while an increase in the proportion of fine aggregates resulted in an increase in the bulk density P. This indicates that the

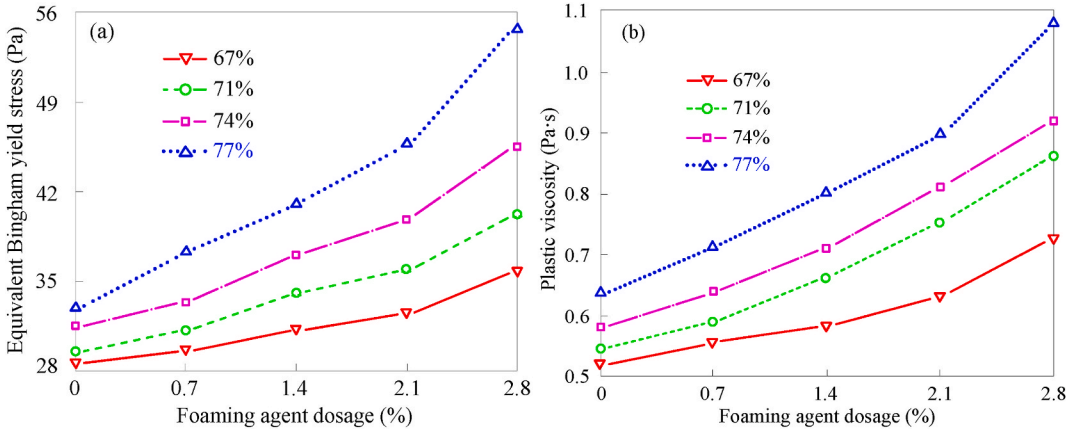

Fig. 6. Influence of foaming agent dosage on the rheological behavior of freshly prepared AASCM.

incorporation of fine particles into the slurry reduced the void spaces between coarse aggregates, leading to an overall increase in the bulk density of the slurry. Furthermore, the range of particle sizes of the foamed filling aggregates was directly proportional to the change in the volume mean diameter, for example, as $D(4,3)$ of the foamed filling aggregates increased from 26.27 μm to 66.82 μm, the particle size distribution width (n) increased from 0.7835 to 0.9052, reflecting the distribution of particle sizes of the foamed filling aggregates became narrower.

Fig. 7 illustrates the effects of foamed filling aggregate's volume mean diameter and bulk density on the flow characteristics of foamed filling slurry. As depicted in the graphical representation 7(a), the fluidity of the foamed filling slurry demonstrates an upward trend as the volume mean diameter increases. This phenomenon can be attributed to the fact that foamed filling aggregates with a smaller volume mean diameter possess a relatively larger specific surface area and require more free water to envelop solid particles, consequently, this reduction in available free water for slurry flow leads to a decrease in fluidity [55]. In addition, the change in fluidity varies with different foam agent dosages. By way of illustration, with a decrease in the volume mean diameter of the filling from 69.05 μm to 26.27 μm, the reduction in fluidity for foaming agent dosages of 0 %, 0.7 %, 1.4 %, 2.1 %, and 2.8 % corresponds to 26.37 %, 23.33 %, 19.55 %, 18.06 %, and 17.24 %, respectively. This can be primarily attributed to the higher foaming agent dosage increases the number of bubbles in the slurry, and similar to solid particles, bubbles will share some free water to form a liquid film, reducing the available water content within the slurry and decreasing fluidity. The higher the foaming agent dosage, the more significant the decrease in fluidity. As shown in Fig. 7(b), the fluidity of foamed filling slurry experiences a substantial reduction as the dosage increases in bulk density. As depicted in Table 2, fine filling have a smaller Rosin Rammler coefficient [56] and a broader range of particle sizes, which increases the bulk density of the material and decreases the gap between solid particles. Upon contact with water, water will first fill the gaps, and then envelop the solid particles, and the remaining free water is used for lubrication and flow between particles [57]. Although the water required for the gaps between solid particles in fine filling is small, the water required for enveloping particles (specific surface area) is large, resulting in a decrease in the overall amount of free water available for particle lubrication and flow.

The effect of filling aggregate size distribution on the equivalent Bingham yield stress (Fig. 8(a)) and plastic viscosity (Fig. 8(b)) of foamed filling slurry is shown in Fig. 8. It is evident that there exists an inverse relationship between the changes in equivalent Bingham yield stress and plastic viscosity and the volumetric mean diameter. This stands in contrast to the trend observed in fluidity. For instance, as the volumetric mean diameter of the aggregate increases from 26.27 μm to 69.05 μm, the equivalent yield stress of foamed filling slurry with foaming agent addition of 0 %, 0.7 %, 1.4 %, 2.1 %, and 2.8 % decreases from 45.65 Pa, 48.74 Pa, 52.21 Pa, 55.28 Pa, and 58.26 Pa–25.77 Pa, 27.60 Pa, 31.02 Pa, 33.51 Pa, and 34.16 Pa, respectively. The corresponding apparent viscosities (Pa·s) also decrease from 1.21, 1.32, 1.45, 1.55, and 1.66 to 0.51, 0.57, 0.64, 0.70, and 0.74. With an increase in the particle size distribution, the interaction between the rise in particle gap and the decrease of specific surface area increases the quantity of unbound water used to lubricate particle flow, thereby reducing the flow resistance, and the value of the equivalent Bingham yield stress and plastic viscosity also decrease accordingly. In addition, it can be seen that the equivalent Bingham yield strength of foamed filling slurry uniformly decreases with increasing particle size, while the plastic viscosity exhibits an initial increase followed by a subsequent decrease. As reported in the research conducted by OUATTARA et al. [58], the shear yield stress of slurry is closely related to extension, but not significantly related to plastic viscosity. Referring to Fig. 8(a), the increment of extension with respect to volumetric mean diameter variation is relatively uniform, which confirms the close correlation between the shear yield stress and extension of foamed filling slurry.

5. Analysis and discussion

Based on the aforementioned experimental findings, it is clear that the foaming agent plays a vital role in shaping the flow properties and rheological behavior of the filling slurry. The presence of bubbles generated by the foaming agent significantly impacts

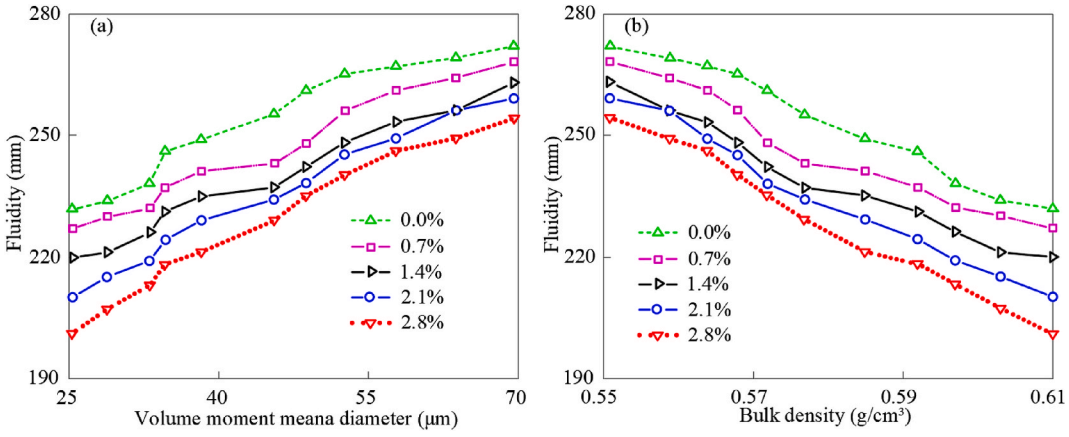

Fig. 7. The influence of aggregate's **a** volume moment mean diameter and **b** bulk density on the fluidity of fresh AASCM.

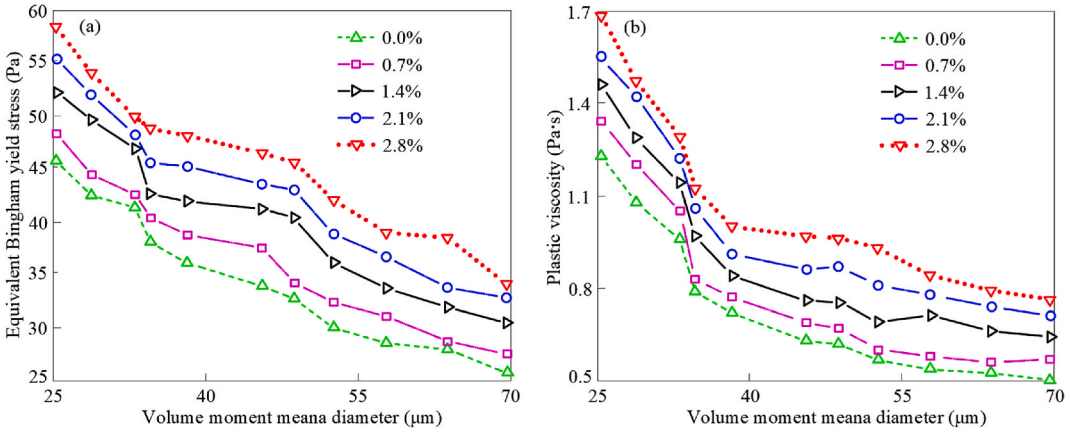

Fig. 8. Impact of particle size on the rheological behavior of fresh AASCM.

the performance of the foamed filling slurry. To systematically analyze the influence of bubbles on the slurry's performance, the WFT theory has been introduced for comprehensive investigation. The WFT theory is commonly used in the field of cement or mortar, which states that the water (W_0) contained in the slurry system can be categorized into two parts: water used for filling voids (W_1) and surplus or additional free water (W_2). The surplus or additional free water surrounds the surface of the solid particles, creating a water film (as depicted in Fig. 9). However, it is important to note that the depicted round shape of GGBFS and gangue particles is an approximation and may not reflect the actual scenario. Similarly, the uniform distribution of excess film thicknesses around the particles shown in the illustration is an unrealistic assumption. If the cumulative quantity of water in the system is lower than or equal to the void filling water, the slump value is very small, and the slurry can be regarded as having no fluidity [59,60]. Therefore, the amount of excess water is the primary condition for the slurry to have fluidity. The specific formula for calculating the thickness of the water film in the slurry is summarized as follows [61]:

$$d_{WFT} = \frac{\mu_W - \mu_S}{A_S}$$

In the equation, A_S represents the specific surface area of the particles. μ_W is the water-to-solid volume ratio, and μ_S is the void ratio calculated from the bulk density (φ).

$$\mu_S = \frac{1-\varphi}{\varphi}$$

Since the distribution of particle sizes of bubbles in the slurry is unknown, it is difficult to obtain the surface area per unit mass of the bubbles. However, after the addition of foaming agent, the expansion ratio of the slurry can be easily obtained experimentally, i.e. the volume fraction of bubble spheres is known. In addition, the bulk density of the mixed system is known through wet measurement. By assuming a particle size distribution for the bubble spheres and mixing them into the solid particle system at a certain volume fraction (determined by the expansion ratio), if the density of the particle packing of the resulting system is consistent with the wet

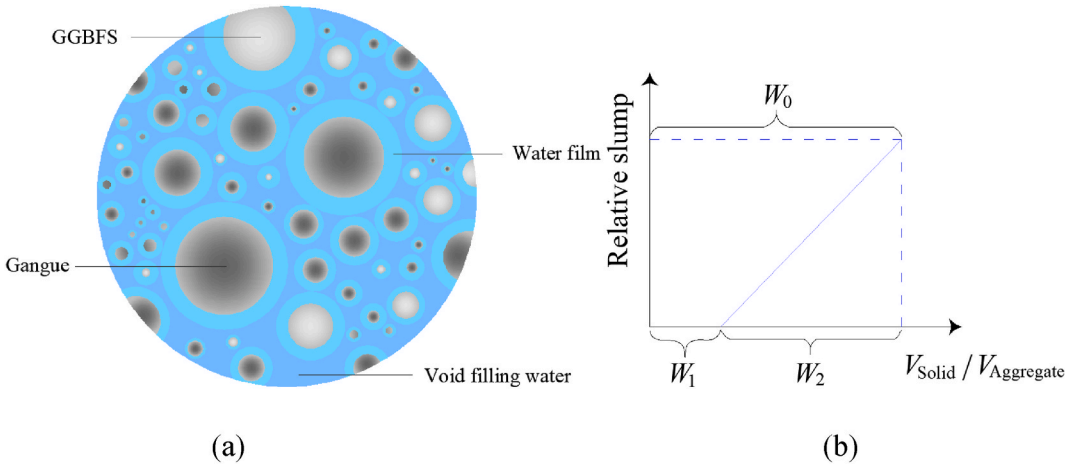

Fig. 9. Diagram depicting (a) water film and (b) correlation between relative slump and water content.

measurement results (achieved through particle flow software PFC^{3D}), the assumption is valid; otherwise, another assumption needs to be made. Based on the final assumption regarding the size of the particles of the bubble spheres, the specific surface area of the system can be further obtained. The specific steps are shown in Fig. 10.

5.1. Stacking simulation error calibration

It is worth noting that there are inevitably errors in estimating bubble size using the method mentioned above. The PFC^{3D} simulation method used in the study employs self-weighted packing, which will inevitably yield a lower packing density than the wet measurement method. If the bubble size calculated using the assumption of equal packing densities is directly utilized for determining the surface area per unit mass, the result would be incorrect. Therefore, it is necessary to calibrate the simulation values with the experimental values to determine the conversion relationship between the two.

In this study, four sizes of gangue samples (100–500 μm) were prepared using vacuum sieving, characterized by the particle size distributions presented in Table 6. The packing densities of each gangue sample were obtained by wet measurement. Subsequently, PFC^{3D} simulations were performed assuming the gangue particles were spherical, and a closed wall of 40 × 40 × 60 (mm) was generated within the effective region. Gangue particles of a specific gradation were then generated within this wall, and under the action of gravity, they were rearranged until a steady-state condition was attained. A linear model was adopted with a particle elastic modulus of 1 GPa, a density of 2.2 g/cm^3, and a friction coefficient of 0.5. Figs. 11 and 12 show the particle model and simulation results of the rearranged gangue, respectively. It should be noted that errors are inevitable when estimating the bubble size using the above method, and that the packing density obtained by gravity packing in PFC^{3D} will be smaller than that obtained by wet measurement. Therefore, it is necessary to calibrate the simulation values with experimental values and establish the conversion relationship between them before calculating the specific surface area.

The packing density obtained by bulk density test is compared with that obtained by PFC^{3D} simulation (Table 7). In light of the findings from both the experiments and simulations, a comparison between the two is presented in Table 7. Observations indicate a consistent underestimation of the simulated values compared to the wet measurement values. This is reasonable since no vibration was applied during the simulation. WONG et al. [49] showed that the tapping process can help to pack fine particles into voids, thereby increasing the packing density. Based on the results, a calibration error coefficient between the simulation and experimental values of around 1.1 was obtained. Therefore, this value can be used to convert the simulation results with the addition of bubbles to the corresponding empirical findings.

5.2. Impact of WFT on the fluidity of foamed filling slurry

Fig. 13 illustrates the relationship between the WFT and the foaming agent dosage. It can be observed that as the foaming agent dosage remains constant, the WFT decreases with an increase in the solid particle concentration, primarily attributed to the reduction in water content. For example, in the case of the foamed backfill slurry with a foaming agent content of 1.4 %, the WFT decreases from 0.588 μm to 0.528 μm as the solid concentration increases from 67 % to 77 %. Additionally, it can be observed that the WFT significantly decreases as the content of the foaming agent is incremented from 0 % to 2.8 %, regardless of the solid particle concentration. The reduction in WFT can primarily be attributed to the combined influence of specific surface area and bulk density. Since

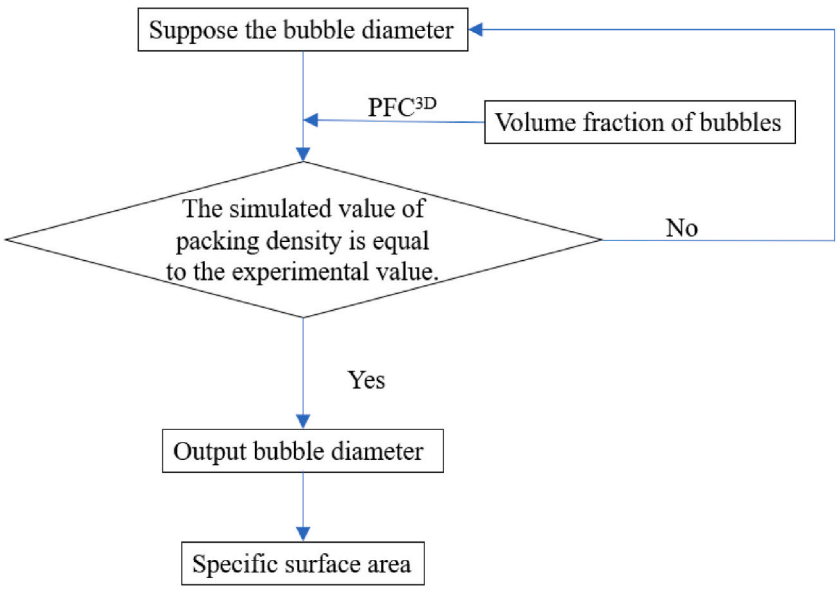

Fig. 10. Calculation process of the specific surface area of system particles.

Table 6
Size range of gangue samples.

Size/μm	Test specimen 1/%	Test specimen 2/%	Test specimen 3/%	Test specimen 4/%
100–150	20.00	30.00	40.00	50.00
150–250	45.32	54.06	59.83	65.28
250–350	71.86	75.17	79.63	82.61
350–500	100.00	100.00	100.00	100.00

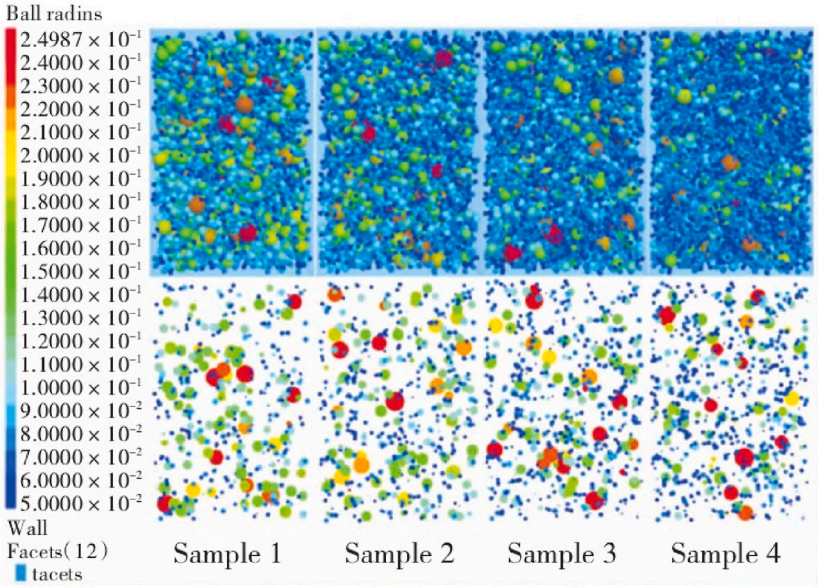

Fig. 11. Particle flow model of packing with different particle size distributions of gangues.

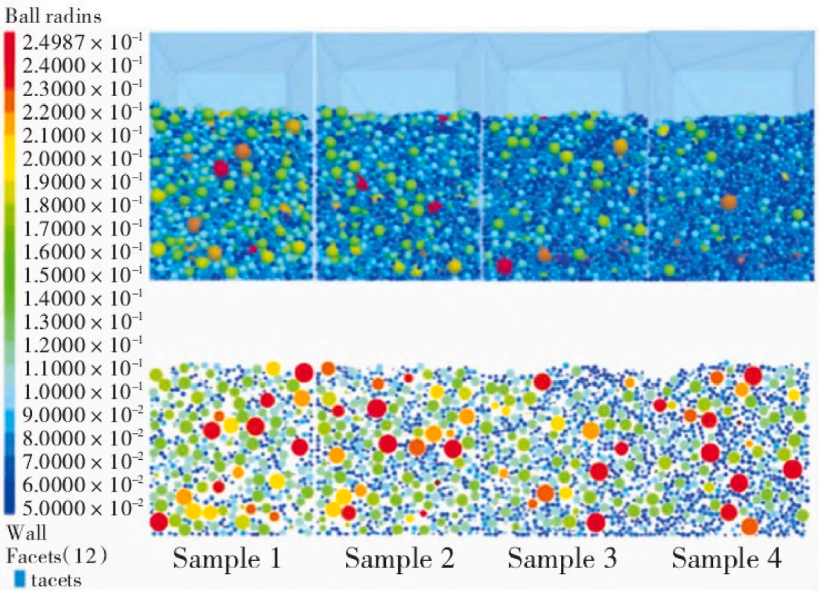

Fig. 12. Packing results of gangue samples.

Table 7
Comparison between modeled and observed packing density.

Measurement	Test specimen 1	Test specimen 2	Test specimen 3	Test specimen 4
Simulation	0.606	0.611	0.616	0.613
Wet packing method	0.662	0.667	0.678	0.682

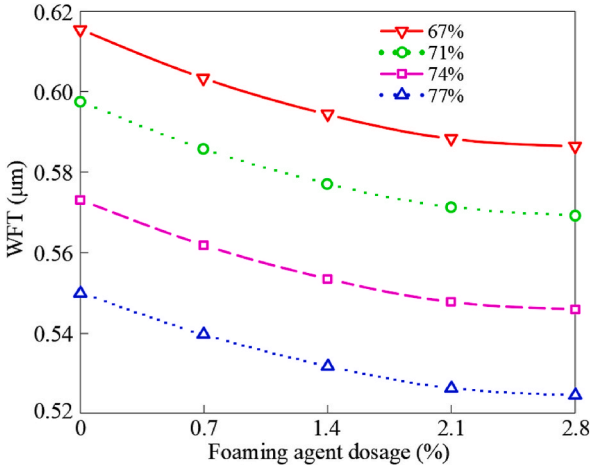

Fig. 13. WFT with foaming agent dosage at different solid contents.

the foaming agent content is relatively small compared to the water content in the slurry, the effect of the foaming agent on the slurry consistency is neglected, i.e., the influence of slurry consistency on bubble stability is not considered. The increase in foaming agent content has two primary effects on the system. Firstly, it results in a higher number of bubbles present in the system. If we consider these bubbles as particles, the addition of foaming agent causes the wet packing system to undergo re-packing, thereby altering the overall bulk density of the system. According to the packing theory [33], mixed particle systems exhibit three physical effects (loose effect, wall effect, and wedging effect) that influence the bulk density. For the slag-gangue-bubble mixture system studied in this paper, the large bubbles act as attachment walls for small particles, and the small bubbles wedge into the gaps between larger-sized particles. Under the combined influence of the wall effect and wedging effect, the void volume of the system increases, and the bulk density decreases. Additionally, the foaming agent produces bubbles with a diameter smaller than the particle size of the gangue employed in the present research, which is equivalent to adding fine filler to the particle system, leading to an increase in the surface area per unit mass of the particles. Therefore, with the increase of foaming agent content, the WFT of the system continues to decrease. It is noteworthy that all WFT values observed in the foamed backfill slurry are greater than zero, indicating an ample presence of water within the system to occupy the void spaces between solid particles. This is also an important difference between backfill and concrete.

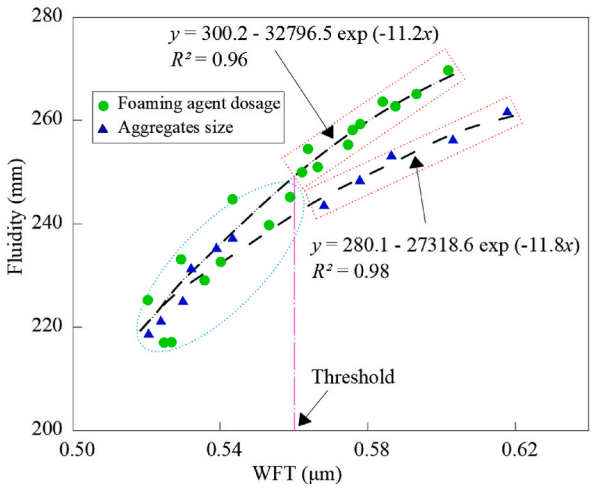

Fig. 14. Relationship between fluidity and WFT.

Negative WFT values often occur in concrete. As depicted in Fig. 13, an increase in foaming agent content leads to an initial rapid decline in WFT, followed by a gradual decrease, regardless of the solid particle concentration. This implies the existence of a saturated foaming agent content from the perspective of WFT. When the foaming agent content reaches this saturation value, the WFT changes are not significant. The magnitude of this value is related to the material properties of the backfill, for instance the particle size of the gangue and the solid particle concentration.

The relationship between fluidity and wall flexural tensile (WFT) is shown in Fig. 14. Generally speaking, the expansion level correlates positively with the growth of WFT. A higher WFT means a stronger lubrication effect between particles, resulting in a decrease in yield stress. Based on the findings of QIU et al. [33], the degree of expansion of the filling slurry is a macroscopic characterization of yield stress. To examine the effect of WFT, the best fitting curve of the expansion-WFT relationship was obtained through regression analysis. Under the condition of keeping the size of the particles of the filling aggregate constant, the expansion of the foamed filling slurry shows an exponential function relationship with WFT, and the fitting correlation coefficient R^2 value is 0.96, indicating that the fluidity of the foamed filling slurry mainly depends on WFT. Importantly, despite the high correlation coefficient, it should be noted that there is a significant difference in the dispersion degree of the data points on either side of the boundary (WFT≈0.56 μm). When WFT>0.56 μm, the foaming agent dosage is about 0 %–2 %. At this time, the data points closely align with the fitting curve, indicating a strong relationship between the degree of expansion and WFT for foamed filling slurries with different foaming agent dosages. This suggests that WFT remains the primary factor influencing the properties of the expanding filling slurry regardless of the foaming agent dosage. However, as WFT decreases below 0.56 μm, corresponding to foaming agent dosages of around 2 %–3 %, the data points start to deviate from the fitting curve. This suggests that at higher foaming agent dosages, WFT alone may no longer be the sole factor controlling the foamed filling slurry, and the influence of the foaming agent dosage itself becomes significant and cannot be disregarded.

In a study investigating the effects of water-reducing agents and their dosages on the rheological and bonding properties of mortar, KWAN et al. [62] explained that the observed phenomenon was caused by the combined direct and indirect effects of water-reducing agents. The indirect effect is attributed to the ability of foaming agents to modify the fluidity of the slurry by influencing the workability factor time (WFT). On the other hand, foaming agents also directly impact the fluidity of the slurry in a way that cannot be solely captured by the WFT parameter. LI et al. [63] suggested that water-reducing agents enhance the fluidity of cement slurries by increasing the WFT and reducing the bonding properties. This reduction in bonding can be considered as a direct effect of water-reducing agents.

By comparing the model proposed in this study with the Kwan model [62], it becomes evident that the flow extension in foamed filling slurry can be represented as a univariate function of WFT, while in concrete mortar, it becomes a bivariate function of WFT and water-reducing agent content. This suggests that, in foamed filling slurry, the direct effect of foaming agents can be somewhat disregarded, and the coupling effect between WFT and foaming agents remains the predominant factor influencing the fluidity of the expanded filling slurry. However, in this particular case, the effect of WFT holds fairly greater significance. This observation can be connected with the higher water content in the filling slurry compared to concrete mortar. Therefore, when the foaming agent dosage is high, the discreteness of the data primarily stems from the direct effect of the foaming agent itself. To simultaneously consider the direct effect of foaming agent dosage and the WFT, a new index, namely, the flocculent membrane thickness (FWFT), proposed by GUO et al. [31], needs to be introduced.

Similarly, when the influencing factor is the aggregate particle size, the WFT and the extension degree also exhibit an exponential relationship, with a correlation coefficient of 0.98. In addition, a threshold WFT also appears with a size of 0.56 μm. Importantly, it should be emphasized that, unlike foaming agents, the agglomeration of aggregates into clusters is the reason for the appearance of the threshold WFT, but fundamentally, it is also influenced by FWFT.

6. Conclusion

This study has experimentally explored the fluidity and rheological properties of AASCM as a function of aggregate gradations and foaming agent dosage. Eleven series of aggregate gradations with volume moment mean diameter (D[3,4]) ranging from 26 to 69 μm were prepared by using fly ash and gangue. AASCM samples with different aggregate gradations and foaming agent dosages (0.0 %, 0.7 %, 1.5 %, 2.3 %, and 3.1 %) were prepared to obtain the slump, plastic viscosity, Bingham yield stress and bulk density of fresh AASCM. The influence mechanism of aggregate gradation and foaming agent dosages on the evolution of fluidity and rheological properties of fresh AASCM was discussed. According to the obtained results, the following conclusions can be drawn:

(1) This paper focuses on investigating the impact of aggregate particle size distribution and foam dosages on the fluidity of AASCM through experimental analysis and uses the PFC^{3D} to build a model of gas-solid particle packing to investigate the evolution law of WFT in foam filling slurries with the increase of expansion degree. The fluidity of AASCM increases with the augmentation of filling aggregate particle size and decreases with the increase of foam dosages. The former exhibits a correlation with the particle voids and specific surface area, while the latter is related to the number and distribution of bubbles in the slurry.
(2) The rheological properties of foam slurries show a negative correlation with the increase of filling the size of the aggregates and increase with the increase of foam dosages. Using the PFC simulation of gas bubble and particle packing models, the error between simulation values and wet measurement experimental values is verified, and the error coefficient is calibrated to 1.1. The WFT of foamed AASCM is estimated using the packing density determined experimentally and the total surface area of the slurry obtained through PFC simulation.

(3) The correlation analysis between the expansion degree and WFT of the slurry shows a correlation coefficient of 0.96 and 0.98, this suggests that the presence of gas bubbles in foamed AASCM alters the overall packing density and specific surface area, thereby affecting their fluidity.

Studying the fluidity and rheological properties of AASCM is an important research field, which can provide a theoretical basis for solving critical issues in underground engineering and infrastructure development.

Additional information

No additional information is available for this paper.

CRediT authorship contribution statement

Kunpeng Yu: Writing – review & editing, Writing – original draft, Project administration, Conceptualization. **Liqiang Ma:** Writing – review & editing, Supervision, Project administration. **Ichhuy Ngo:** Conceptualization. **Yangyang Wang:** Validation, Resources, Methodology. **Jiangtao Zhai:** Software, Formal analysis.

Declaration of competing interest

The authors declare that they have no known competing financial interests or personal relationships that could have appeared to influence the work reported in this paper.

Acknowledgments

The authors would like to make an appreciation to the Fundamental Research Funds for the Central Universities (2022QN1004) for financial support.

References

[1] Zhi Cao, Rupert J. Myers, Richard C. Lupton, Huabo Duan, Romain Sacchi, Nan Zhou, T. Reed Miller, Jonathan M. Cullen, Quansheng Ge, Gang Liu, The sponge effect and carbon emission mitigation potentials of the global cement cycle, Nat. Commun. 11 (1) (2020) 3777, https://doi.org/10.1038/s41467-020-17583-w.
[2] G. Habert, S.A. Miller, V.M. John, J.L. Provis, A. Favier, A. Horvath, K.L. Scrivener, Environmental impacts and decarbonization strategies in the cement and concrete industries, Nat. Rev. Earth Environ. 1 (11) (2020) 559–573, https://doi.org/10.1038/s43017-020-0093-3.
[3] Rashid Rehan, Moncef Nehdi, Carbon dioxide emissions and climate change: policy implications for the cement industry, Environ. Sci. Pol. 8 (2) (2005) 105–114, https://doi.org/10.1016/j.envsci.2004.12.006.
[4] Jabulani Matsimbe, Megersa Dinka, David Olukanni, Innocent Musonda, A Bibliometric analysis of research trends in geopolymer, Materials 15 (2022) 6979, https://doi.org/10.3390/ma15196979.
[5] Hasanbeigi Ali, Lynn Price, Elina Lin, Emerging energy-efficiency and CO2 emission-reduction technologies for cement and concrete production: a technical review, Renew. Sustain. Energy Rev. 16 (8) (2012) 6220–6238, https://doi.org/10.1016/j.rser.2012.07.019.
[6] Chinyere O. Nwankwo, Gideon O. Bamigboye, Iyinoluwa E.E. Davies, Temitope A. Michaels, High volume Portland cement replacement: a review, Constr. Build. Mater. 260 (2020), 120445, https://doi.org/10.1016/j.conbuildmat.2020.120445.
[7] Xueyuan Lv, Hao Cheng, Pang Chen, Yonggan Li, Zhiyong Wang, Influence of high temperature on the compression and bending properties of AASCM, Mag. Concr. Res. (2023) 1–44, https://doi.org/10.1680/jmacr.23.00029.
[8] Hao Cheng, Pang Chen, Xian Rong, Shaojun Cao, Wenzhong Zhao, Effect of steel fibre and manufactured sand on mechanical properties of alkali-activated slag green cementitious material after high temperature, Case Stud. Constr. Mater. 18 (2023), e01919, https://doi.org/10.1016/j.cscm.2023.e01919.
[9] Ismail Amer, Kohail Mohamed, El-Feky, M.S. El-Feky, Rashad Ahmed, Mohamed A. Khalaf, Characterization of alkali-activated hybrid slag/cement concrete, Ain Shams Eng. J. 12 (1) (2021) 135–144, https://doi.org/10.1016/j.asej.2020.08.003.
[10] Chao Li, Henghu Sun, Longtu Li, A review: the comparison between alkali-activated slag (Si+ Ca) and metakaolin (Si+ Al) cements, Cement Concr. Res. 12 (40) (2010) 1768, https://doi.org/10.1016/j.cemconres.2010.03.020.
[11] Hao Cheng, Pang Chen, Shaojun Cao, Yunhe Li, Stress–strain model of steel fibre-reinforced alkali-activated slag cementitious material after high-temperature exposure, J. Build. Eng. (2023), 107743, https://doi.org/10.1016/j.jobe.2023.107743.
[12] Zhongzhe Zhang, Yongsheng Ji, Zhanguo Ma, Furong Gao, Mingming Ma, Zhishan Xu, Effect of polyacrylamide on rheological properties of underwater non-dispersible paste of alkali-activated slag, KSCE J. Civ. Eng. 26 (1) (2022) 236–247, https://doi.org/10.1007/s12205-021-0090-1.
[13] Divya Khale, Rubina Chaudhary, Mechanism of geopolymerization and factors influencing its development: a review, J. Mater. Sci. 42 (2007) 729–746, https://doi.org/10.1007/s10853-006-0401-4.
[14] Hengels Castillo, Humberto Collado, Thomas Droguett, Sebastián Sánchez, Mario Vesely, Pamela Garrido, Sergio Palma, Factors affecting the compressive strength of geopolymers: a review, Minerals 11 (12) (2021) 1317, https://doi.org/10.3390/min11121317.
[15] Bibhuti Bhusan Mukharjee & Rakesh Kumar Patra, Effect of coarse recycled aggregate and rice husk ash on concrete: a factorial design approach, Iran. J. Sci. Technol.-Trans. Civ. Eng. 46 (6) (2022) 4169–4185, https://doi.org/10.1007/s40996-022-00856-3.
[16] J. Duchesne, Alternative supplementary cementitious materials for sustainable concrete structures: a review on characterization and properties, Waste Biomass Valorization 12 (2021) 1219–1236, https://doi.org/10.1007/s12649-020-01068-4.
[17] Nancy A. Soliman, Arezki Tagnit-Hamou, Partial substitution of silica fume with fine glass powder in UHPC: filling the micro gap, Constr. Build. Mater. 139 (2017) 374–383, https://doi.org/10.1016/j.conbuildmat.2017.02.084.
[18] M.B. Mohd Salahuddin, M. Norkhairunnisa, F. Mustapha, A review on thermophysical evaluation of alkali-activated geopolymers, Ceram. Int. 41 (3) (2015) 4273–4281, https://doi.org/10.1016/j.ceramint.2014.11.119.
[19] Alaa M. Rashad, Alkali-activated metakaolin: a short guide for civil Engineer–An overview, Constr. Build. Mater. 41 (2013) 751–765, https://doi.org/10.1016/j.conbuildmat.2012.12.030.
[20] Jagmeet Singh, S.P. Singh, Geopolymerization of solid waste of non-ferrous metallurgy–A review, J. Environ. Manage. 251 (2019), 109571, https://doi.org/10.1016/j.jenvman.2019.109571.
[21] Fernando Pacheco-Torgal, João Castro-Gomes, Jalali Said, Alkali-activated binders: a review: Part 1. Historical background, terminology, reaction mechanisms and hydration products, Constr. Build. Mater. 22 (7) (2008) 1305–1314, https://doi.org/10.1016/j.conbuildmat.2007.10.015.

[22] Kostas Komnitsas, Dimitra Zaharaki, Geopolymerisation: a review and prospects for the minerals industry, Miner. Eng. 20 (14) (2007) 1261–1277, https://doi.org/10.1016/j.mineng.2007.07.011.

[23] Qifei Huang, Qi Wang, Dong Lu, Beidou Xi, Binyan Zhou, The current situation of solid waste management in China, J. Mater. Cycles Waste Manag. 8 (2006) 63–69, https://doi.org/10.1007/s10163-005-0137-2.

[24] S.K. Behera, D.P. Mishra, Prashant Singh, K. Mishra, Sujit K. Mandal, C.N. Ghosh, Ritesh Kumar, Phanil K. Mandal, Utilization of mill tailings, fly ash and slag as mine paste backfill material: review and future perspective, Constr. Build. Mater. 309 (2021), 125120, https://doi.org/10.1016/j.conbuildmat.2021.125120.

[25] Jixiong Zhang, Li Meng, Abbas Taheri, Weiqing Zhang, Zhongya Wu, Weijian Song, Properties and application of backfill materials in coal mines in China, Minerals 9 (1) (2019) 53, https://doi.org/10.3390/min9010053.

[26] Longjun Dong, Xiaojie Tong, Xibing Li, Jian Zhou, Shaofeng Wang, Bing Liu, Some developments and new insights of environmental problems and deep mining strategy for cleaner production in mines, J. Clean. Prod. 210 (2019) 1562–1578, https://doi.org/10.1016/j.jclepro.2018.10.291.

[27] Xinguo Zhang, Lin Jia, Jinxiao Liu, Fei Li, Zhenzhong Pang, Investigation of hydraulic-mechanical properties of paste backfill containing coal gangue-fly ash and its application in an underground coal mine, Energies 10 (9) (2017) 1309, https://doi.org/10.3390/en10091309.

[28] Naguleswaran Niroshan, Nagaratnam Sivakugan, Ryan Llewellyn Veenstra, Flow characteristics of cemented paste backfill, Geotech. Geol. Eng. 36 (4) (2018) 2261–2272, https://doi.org/10.1007/s10706-018-0460-8.

[29] Yang Pan, Lang Liu, Yonglu Suo, Geng Xie, Weiji Sun, Caixin Zhang, Physical-chemical coupling excitation of low activity coal gasification slag solid waste and its application as a backfill cementitious material, Constr. Build. Mater. 401 (2023), 132973, https://doi.org/10.1016/j.conbuildmat.2023.132973.

[30] Lei Yang, Erol Yilmaz, Junwei Li, Hui Liu, Haiqiang Jiang, Effect of superplasticizer type and dosage on fluidity and strength behavior of cemented tailings backfill with different solid contents, Constr. Build. Mater. 187 (2018) 290–298, https://doi.org/10.1016/j.conbuildmat.2018.07.155.

[31] Zhenbang Guo, Jingping Qiu, Haiqiang Jiang, Jun Xing, Xiaogang Sun, Zhengyu Ma, Flowability of ultrafine-tailings cemented paste backfill incorporating superplasticizer: insight from water film thickness theory, Powder Technol. 381 (2021) 509–517, https://doi.org/10.1016/j.powtec.2020.12.035.

[32] Jingping Qiu, Zhenbang Guo, Lei Yang, Haiqiang Jiang, Yingliang Zhao, Effects of packing density and water film thickness on the fluidity behaviour of cemented paste backfill, Powder Technol. 359 (2020) 27–35, https://doi.org/10.1016/j.powtec.2019.10.046.

[33] Jingping Qiu, Zhenbang Guo, Lei Yang, Haiqiang Jiang, Yingliang Zhao, Effect of tailings fineness on flow, strength, ultrasonic and microstructure characteristics of cemented paste backfill, Constr. Build. Mater. 263 (2020), 120645, https://doi.org/10.1016/j.conbuildmat.2020.120645.

[34] A. Hallal, E.H. Kadri, K. Ezziane, A. Kadri, H. Khelafi, Combined effect of mineral admixtures with superplasticizers on the fluidity of the blended cement paste, Constr. Build. Mater. 24 (8) (2010) 1418–1423, https://doi.org/10.1016/j.conbuildmat.2010.01.015.

[35] Chiara F. Ferraris, Karthik H Obla, Russell Hill, The influence of mineral admixtures on the rheology of cement paste and concrete, Cement Concr. Res. 31 (2) (2001) 245–255, https://doi.org/10.1016/S0008-8846(00)00454-3.

[36] Jun Wu, Li Liu, Yongfeng Deng, Guoping Zhang, Annan Zhou, Qiong Wang, Distinguishing the effects of cementation versus density on the mechanical behavior of cement-based stabilized clays, Constr. Build. Mater. 271 (2021), 121571, https://doi.org/10.1016/j.conbuildmat.2020.121571.

[37] Li Xiang, Dawei Cui, Yuan Zhao, Ruoxiang Qiu, Xuemin Cui, Kaituo Wang, Preparation of high-performance thermal insulation composite material from alkali-activated binders, foam, hollow glass microspheres and aerogel, Constr. Build. Mater. 346 (2022), 128493, https://doi.org/10.1016/j.conbuildmat.2022.128493.

[38] Giulia Masi, William D.A. Rickard, Les Vickers, Maria Chiara Bignozzi, Arie van Riessen, A comparison between different foaming methods for the synthesis of light weight geopolymers, Ceram. Int. 40 (9) (2014) 13891–13902, https://doi.org/10.1016/j.ceramint.2014.05.108.

[39] V. Ducman, L. Korat, Characterization of geopolymer fly-ash based foams obtained with the addition of Al powder or H2O2 as foaming agents, Mater. Charact. 113 (2016) 207–213, https://doi.org/10.1016/j.matchar.2016.01.019.

[40] Drissa Ouattara, Ammar Yahia, Mamert Mbonimpa, Tikou Belem, Effects of superplasticizer on rheological properties of cemented paste backfills, Int. J. Miner. Process. 161 (2017) 28–40, https://doi.org/10.1016/j.minpro.2017.02.003.

[41] Drissa Ouattara, Tikou Belem, Mamert Mbonimpa, Ammar Yahia, Effect of superplasticizers on the consistency and unconfined compressive strength of cemented paste backfills, Constr. Build. Mater. 181 (2018) 59–72, https://doi.org/10.1016/j.conbuildmat.2018.05.288.

[42] ASTM C143, Standard Test Method for Slump of Hydraulic-Cement Concrete, Book of ASTM Standards, 2015.

[43] Ester Galicia-Aldama, Miguel Mayorga, Juan Carlos Arteaga-Arcos, Lorena Romero-Salazar, Rheological behaviour of cement paste added with natural fibres, Constr. Build. Mater. 198 (2019) 148–157, https://doi.org/10.1016/j.conbuildmat.2018.11.179.

[44] R.P. Chhabra, J.F. Richardson, Non-Newtonian Fluid Behaviour. Non-newtonian Flow and Applied Rheology, 2008, pp. 1–55.

[45] I. Iskhakov, Y. Ribakov, Ultimate limit state of pre-stressed reinforced concrete elements, Mater. Des. 75 (2015) 9–16, https://doi.org/10.1016/j.matdes.2015.02.020.

[46] Wen-bin Liu, Xiong Zhang, Study on volume stability of chemical foaming cement paste, KSCE J. Civ. Eng. 21 (2017) 2790–2797, https://doi.org/10.1007/s12205-017-0985-z.

[47] L.G. Li, A.K.H. Kwan, Packing density of concrete mix under dry and wet conditions, Powder Technol. 253 (2014) 514–521, https://doi.org/10.1016/j.powtec.2013.12.020.

[48] Ming Zhao, Xiong Zhang, Yongjuan Zhang, Effect of free water on the flowability of cement paste with chemical or mineral admixtures, Constr. Build. Mater. 111 (2016) 571–579, https://doi.org/10.1016/j.conbuildmat.2016.02.057.

[49] Henry H.C. Wong, Albert K.H. Kwan, Packing density of cementitious materials: part 1—measurement using a wet packing method, Mater. Struct. 41 (2008) 689–701, https://doi.org/10.1617/s11527-007-9274-5.

[50] S. Choudhury, T. Jena, Influence of surfactant on foam generation and stabilization in cement slurry, Mater. Today: Proc. (2023), https://doi.org/10.1016/j.matpr.2023.07.266.

[51] Min Xiao, Fangxian Li, Pengfei Yang, Bin Li, Jiangxiong Wei, Qijun Yu, Influence of slurry characteristics on the bubble stability in foamed concrete, J. Build. Eng. 71 (2023), 106500, https://doi.org/10.1016/j.jobe.2023.106500.

[52] E.K. Kunhanandan Nambiar, K. Ramamurthy, Air-void characterisation of foam concrete, Cement Concr. Res. 37 (2007) 221–230, https://doi.org/10.1016/j.cemconres.2006.10.009.

[53] X.J. Deng, B. Klein, D.J. Hallbom, B. de Wit, J.X. Zhang, Influence of particle size on the basic and time-dependent rheological behaviors of cemented paste backfill, J. Mater. Eng. Perform. 27 (2018) 3478–3487, https://doi.org/10.1007/s11665-018-3467-7.

[54] Xuejie Deng, Jixiong Zhang, Bern Klein, Nan Zhou, deWit Benjamin, Experimental characterization of the influence of solid components on the rheological and mechanical properties of cemented paste backfill, Int. J. Miner. Process. 168 (2017) 116–125, https://doi.org/10.1016/j.minpro.2017.09.019.

[55] Huan Ye, Xiaojian Gao, Rui Wang, Hui Wang, Relationship among particle characteristic, water film thickness and flowability of fresh paste containing different mineral admixtures, Constr. Build. Mater. 153 (2017) 193–201, https://doi.org/10.1016/j.conbuildmat.2017.07.093.

[56] A.K.H. Kwan, H.H.C. Wong, Effects of packing density, excess water and solid surface area on flowability of cement paste, Adv. Cem. Res. 20 (1) (2008) 1–11, https://doi.org/10.1680/adcr.2008.20.1.1.

[57] W.W.S. Fung, A.K.H. Kwan, H.H.C. Wong, Wet packing of crushed rock fine aggregate, Mater. Struct. 42 (2009) 631–643, https://doi.org/10.1617/s11527-008-9409-3.

[58] Drissa Ouattara, Mamert Mbonimpa, Ammar Yahia, Tikou Belem, Assessment of rheological parameters of high density cemented paste backfill mixtures incorporating superplasticizers, Constr. Build. Mater. 190 (2018) 294–307, https://doi.org/10.1016/j.conbuildmat.2018.09.066.

[59] Y. Ghasemi, M. Emborg, A. Cwirzen, Effect of water film thickness on the flow in conventional mortars and concrete, Mater. Struct. 52 (2019) 1–15, https://doi.org/10.1617/s11527-019-1362-9.

[60] Y. Ghasemi, M. Emborg, A. Cwirzen, Exploring the relation between the flow of mortar and specific surface area of its constituents, Constr. Build. Mater. 211 (2019) 492–501, https://doi.org/10.1016/j.conbuildmat.2019.03.260.

[61] A.K.H. Kwan, M. McKinley, Effects of limestone fines on water film thickness, paste film thickness and performance of mortar, Powder Technol. 261 (2014) 33–41, https://doi.org/10.1016/j.powtec.2014.04.027.
[62] Albert K.H. Kwan, Jia Jian Chen, Roles of packing density and water film thickness in rheology and strength of cement paste, J. Adv. Concr. Technol. 10 (10) (2012) 332–344, https://doi.org/10.3151/jact.10.332.
[63] Leo G. Li, Albert K.H. Kwan, Effects of superplasticizer type on packing density, water film thickness and flowability of cementitious paste, Constr. Build. Mater. 86 (2015) 113–119, https://doi.org/10.1016/j.conbuildmat.2015.03.104.